

AD-A196 547

2

DTIC FILE COPY

SACLANTCEN REPORT
serial no.: SR-138

SACLANT ASW
RESEARCH CENTRE
REPORT



Passive localization:
A model-based approach

J.V. Candy and
Sullivan

DTIC
ELECTE
S JUN 30 1988 D
E

May 1988

The SACLANT ASW Research Centre provides the Supreme Allied Commander Atlantic (SACLANT) with scientific and technical assistance under the terms of its NATO charter, which entered into force on 1 February 1963. Without prejudice to this main task—and under the policy direction of SACLANT—the Centre also renders scientific and technical assistance to the individual NATO nations.

This document has been approved
for public release and sale in
distribution is unlimited.

88 6 29 171

This document is released to a NATO Government at the direction of SACLANT ASW Research Centre subject to the following conditions:

- The recipient NATO Government agrees to use its best endeavours to ensure that the information herein disclosed, whether or not it bears a security classification, is not dealt with in any manner (a) contrary to the intent of the provisions of the Charter of the Centre, or (b) prejudicial to the rights of the owner thereof to obtain patent, copyright, or other like statutory protection therefor.
- If the technical information was originally released to the Centre by a NATO Government subject to restrictions clearly marked on this document the recipient NATO Government agrees to use its best endeavours to abide by the terms of the restrictions so imposed by the releasing Government.

Page count for SR-138
(excluding covers)

Pages	Total
i-iv	4
1-38	38
	<hr/>
	42

SACLANT ASW Research Centre
Viale San Bartolomeo 400
19026 San Bartolomeo (SP), Italy

tel: 0187 540 111
telex: 271148 SACENT I

NORTH ATLANTIC TREATY ORGANIZATION

SACLANTCEN SR-138

Passive localization:
A model-based approach

J.V. Candy and E.J. Sullivan

The content of this document pertains
to *work performed under Project 02* of
the SACLANTCEN Programme of Work
The document has been approved for
release by The Director, SACLANTCEN.



Peter C. Wille
Director

SACLANTCEN SR-138

- ii -

intentionally blank page

**Passive localization:
A model-based approach**

J.V. Candy and E.J. Sullivan

acoustic *signature*

Abstract: Passive localization by use of propagation models, sometimes called 'Matched Field Processing' is usually carried out in three steps. First some appropriate model is selected, then model parameters (usually taken from archival data or from auxiliary measurements) are introduced into the model. Finally acoustic measurements of the field radiated by the source to be located are made - which, in combination with the properly parameterized model, allow a solution for the source coordinates to be carried out. Here we use such a model-based approach in conjunction with a normal-mode model. By coupling the procedure with a parameter estimation/identification scheme and using a horizontal (towed) array instead of the usual vertical array, we show that the model parameters need not be known *a priori* in order to carry out the solution. This is in contrast to the standard approach in which the modal functions and wavenumber must be *a priori* known in order to solve the problem; sufficient information to determine the range of the source can be inferred directly from the measured data themselves. Using a sophisticated acoustic propagation model to generate simulated data, coupled with various array processing techniques, the feasibility of the approach is demonstrated. The essential problems associated with the technique are found to be (1) the need for a large aperture for sufficiently accurate wavenumber estimation, and (2) the need for a general sensitivity study in order to evaluate the efficiency of the algorithm.

Keywords: acoustic propagation model ◦ array signal processing ◦ beamforming ◦ model-based approach ◦ normal modes ◦ optimal constrained estimation ◦ range estimation ◦ wavenumber estimation.

Accession For	
NTIS GRA&I	<input checked="" type="checkbox"/>
DTIC TAB	<input type="checkbox"/>
Unannounced	<input type="checkbox"/>
Justification	
By	
Distribution/	
Availability Codes	
Dist	Avail and/or Special
A-1	



Contents

1. Introduction 1
2. Propagation and measurement models 4
3. Processor design 11
4. Simulation results 17
5. Summary and recommendations 25

References 27

Appendix A - MATLAB implementation of the algorithm 29

Acknowledgement: The content of this document pertains to work performed under partial support from the Office of the Chief of Naval Research, ONR Contract N00014-87-F-0114, and the Lawrence Livermore National Laboratory under auspices of the US Department of Energy, DOE Contract W-7405-ENG-48.

1. Introduction

The utilization of propagation models to localize sources is well established [1-6]. Most techniques rely on experimental measurements (e.g. of sound velocity profile) to establish model parameters. Applications of these techniques evolve from seismics (where it is used for the location of earthquake epicentres or underground explosions) radar (for target location), and acoustics (for sonar source localization). Here we concentrate on the acoustics application.

The localization of an acoustic source using measured data in conjunction with a propagation model is usually referred to as Matched Field Processing and has been receiving increasing attention in recent years. The technique involves bringing measured acoustic data, most commonly from a vertical array, into consistency with the prediction of a propagation model. The source coordinates are then taken to be those that best match the data.

There are generally two approaches to the problem. The first involves a search over forward solutions to the propagation model. It was in this approach that the term Matched Field Processing was first applied. It is best described as the solution to an inverse problem by forward modeling. Suppose the range and depth of a point acoustic source are to be estimated from the data received on a vertical array of hydrophones. The field at the array, as predicted for a source location at some arbitrary point on the range-depth grid, is computed for an exhaustive set of those points. Each of these computed fields is then compared to the measured field in some manner. For example, the estimator could be the correlation between the measured and the predicted field. This estimator is then computed for all range-depth combinations and plotted on a range-depth map. The location of the best estimate on this map is then taken as the estimate of the location of the source.

One example of such an estimator is Bucker's Detection Factor [2]. This can be written as

$$D(\{\alpha\}) = P_M^H(\{\alpha\}) \mathbf{R} P_M(\{\alpha\}), \quad (1.1)$$

where \mathbf{R} is the covariance matrix of the measured field, $P_M(\{\alpha\})$ is the field as predicted by the model for source coordinates $\{\alpha\}$, and P_M^H is the complex conjugate transpose.

For a vertical array of L hydrophones, $P_M(\{\alpha\})$ is an L -dimensional complex vector and \mathbf{R} is $L \times L$. (It should be noted here that in Bucker's original definition the diagonal of \mathbf{R} is removed.) Equation (1.1) can be thought of as the power output of a conventional beamformer 'steering vector' $P_M(\{\alpha\})$.

The detection factor is maximum when the modeled field equates to the measured field. This can be seen as follows. Assuming that the estimate of the covariance matrix is obtained by a time average $\langle \dots \rangle$, we have

$$D = P_M^t \mathbf{R} P_M = P_M^t \langle P P^t \rangle P_M, \quad (1.2)$$

where we have dropped the explicit dependence on $\{\alpha\}$ for clarity. Since P_M is deterministic (for the case of a deterministic model), Eq. (1.2) can be written as

$$D = \langle P_M^t P P^t P_M \rangle = \langle (P_M^t P) (P_M^t P)^t \rangle. \quad (1.3)$$

By the Schwartz inequality the inner product $P_M^t P$ is maximum when $c P_M = P$, where c is a constant.

Other estimators have been used but most are basically a modification of Eq. (1.1). The disadvantage of this approach is the scale of the computation involved. However, this is outweighed in many situations by the fact that there is no limitation on the degree of sophistication of the model, since only forward solutions are used.

The second approach, known as the direct inversion technique, is based on the fact that the normal-mode model of propagation permits a set of linear equations that can be directly inverted [3, 6].

A more complete overview of these techniques can be found in [3]. Both of these techniques are therefore model-based processing schemes that contain three components: data, model and model parameters. The model parameters are usually derived from a secondary set of measurements or from archival data. The procedure, then, would be to select a model that can be assumed to faithfully represent the physics of the situation. Next some 'best' set of parameters is determined, either by an auxiliary measurement or, more commonly, from archival data. In the case of the normal-mode model these parameters include the sound velocity profile, the depth of the ocean, and the ocean bottom conditions. The parameterized model is then used in conjunction with the measured data, usually from a vertical array, to compute the source location.

In this report we present a technique that differs from the above approaches in two ways. Firstly, a horizontal (towed) array is used to perform the measurements. Secondly, the necessary model parameter information is estimated directly from the data. Thus we have a scheme that is best described as model-based processing with identification [10]. The array data are spectrally analysed spatially by a 'beam-former' which can be of any type (i.e. conventional, maximum-entropy, etc.), and from which the wavenumbers associated with the normal-mode model are estimated. Given these wavenumber estimates, the array measurement data can then be used to provide a direct estimate of the range of the source. What is surprising is that the sound velocity profile, the ocean depth and the bottom properties are not necessary.

SACLANTCEN SR-138

In other words, the horizontal wavenumbers carry sufficient information concerning these parameters to provide a solution. The technique developed follows an eigenvector decomposition approach [12-14].

In Sect. 2 we briefly summarize the propagation and measurement models using the processor. The wavenumber eigentechnique is developed along with the range estimator in Sect. 3. In Sect. 4 we discuss the results on simulated data and summarize the results in Sect. 5.

2. Propagation and measurement models

Acoustic energy from a point source propagating over a long range r ($r \gg h$ where h is depth) towards a receiver can be modeled as a trapped wave characterized by a waveguide phenomenon. For a layered waveguide model with sources on the z (or vertical) axis, the pressure field p is symmetric about z and therefore is governed by the cylindrical wave equation, which is given by

$$\frac{\partial^2}{\partial r^2} p(r, z, t) + \frac{1}{r} \frac{\partial}{\partial r} p(r, z, t) + \frac{\partial^2}{\partial z^2} p(r, z, t) - \frac{1}{c^2} \frac{\partial^2}{\partial t^2} p(r, z, t). \quad (2.1)$$

The solution to this equation is accomplished by using the separation of variables technique, i.e.

$$p(r, z, t) = u(r)\phi(z)T(t). \quad (2.2)$$

Substituting Eq. (2.2) into Eq. (2.1), assuming a harmonic source, we have

$$T(t) = e^{j\omega t} \quad (2.3)$$

And defining separation constants κ_z , κ_r , we obtain the set of equations

$$\frac{d^2}{dr^2} u(r) + \frac{1}{r} \frac{d}{dr} u(r) = -\kappa_r^2 u(r), \quad (2.4)$$

$$\frac{d^2}{dz^2} \phi(z) = -\kappa_z^2 \phi(z), \quad (2.5)$$

$$\kappa^2 = \frac{\omega^2}{c^2(z)}, \quad (2.6)$$

$$\kappa^2 = \kappa_r^2 + \kappa_z^2, \quad (2.7)$$

where the solutions to these relations describe the propagation of the acoustic pressure in cylindrical coordinates, assuming the harmonic source of Eq. (2.3) and the speed of sound a function of depth $c = c(z)$.

Following Clay and Medwin [7], the solution to the range-dependent relation of Eq. (2.4) is given by the approximation to a cylindrical Bessel function as

$$u(r) = \frac{1}{\sqrt{2\pi r}} e^{j(\kappa_r r - \pi/4)} \quad (2.8)$$

which shows that the waves spread radially from the source and are attenuated by $1/\sqrt{r}$.

The depth relation of Eq. (2.5) is an eigenvalue equation in z with

$$\frac{\partial^2}{\partial z^2} \phi_m(z) + \kappa_z(m) \phi_m(z) = 0, \quad m = 1, \dots, N, \quad (2.9)$$

whose eigensolutions $\{\phi_m(z)\}$ are the so-called *modal functions* and κ_z is the wavenumber in the z -direction. These solutions obviously depend on the sound velocity profile $c(z)$ and the boundary conditions at the surface and bottom.

Using the orthogonality property of the modal functions [7], i.e.

$$\int_0^h \rho_0 \phi_m(z) \phi_n(z) dz = \nu_m \delta(m - n), \quad (2.10)$$

with ρ_0 the water density and ν_m a normalization factor for a point source located at z_s , we can expand the source depth pressure dependence on z as a sum of eigenfunctions given by

$$\delta(z - z_s) = \sum_{m=1}^N \left(\frac{\rho_0 \phi_m(z_s)}{\nu_m} \right) \phi_m(z). \quad (2.11)$$

Coupling these solutions to the dispersion relation of Eq. (2.7), we obtain the total wavenumber as

$$\kappa^2(m) = \frac{\omega^2}{c^2(z)} = \kappa_r^2(m) + \kappa_z^2(m), \quad m = 1, \dots, N, \quad (2.12)$$

where κ_r and κ_z are the respective wavenumbers in the r - and z -directions, c is the depth-dependent sound velocity profile, and ω is the harmonic source frequency.

If we also incorporate propagation losses (in the r -direction), then the model wavenumbers become complex with $\kappa_r \rightarrow \kappa_r + j\alpha_r$ in Eq. (2.8). The solution of the wave equation with boundary conditions is the product of Eq. (2.2) and the acoustic pressure is the sum over all modes as given by [7]:

$$p(r, z, t) = a_0 e^{j(\omega t - \pi/4)} \sum_{m=1}^N \frac{\rho_0 \phi_m(z_s) \phi_m(z)}{\nu_m \sqrt{2\pi \kappa_r(m) r}} e^{-\alpha_r(m)r} e^{j\kappa_r(m)r}. \quad (2.13)$$

Here a_0 is the source strength.

For our purpose we are concerned with the localization of the source, and therefore we remove the time dependence, normalize units, and obtain the *acoustic pressure propagation model*¹

¹ A more detailed description of this model, which is used for simulation purposes in Sect. 4, is given in [15].

$$p(r, z) = \sum_{m=1}^N \phi_m(z_s) \phi_m(z) \frac{e^{-\alpha_r(m)r}}{\sqrt{\kappa_r(m)r}} e^{j\kappa_r(m)r}, \quad (2.14)$$

where p is the acoustic pressure, ϕ_m is the m th modal function at z and z_s , $\kappa_r(m)$ is the horizontal wavenumber for the m th mode and r is the horizontal range. In vector form this is

$$p(r, z) = [e^{j\kappa_r(1)r} \dots e^{j\kappa_r(N)r}] \begin{bmatrix} \phi_1(z_s) \phi_1(z) e^{-\alpha_r(1)r / \sqrt{\kappa_r(1)r}} \\ \vdots \\ \phi_N(z_s) \phi_N(z) e^{-\alpha_r(N)r / \sqrt{\kappa_r(N)r}} \end{bmatrix} \quad (2.15)$$

or

$$p(r, z) = \underline{d}'(\tau) \underline{\phi}(r, z). \quad (2.16)$$

We will assume that the acoustic pressure is sampled horizontally through an array of L sensors as shown in Fig. 1. The total range from the source to the i th sensor is given by

$$\rho_i = r_s + r_i,$$

where r_i is the horizontal sensor location and r_s is the range to the first hydrophone (i.e. the hydrophone closest to the source). Substituting ρ_i for r in the propagation model and using this relation, we have

$$p(\rho_i, z) = \sum_{m=1}^N \phi_m(z_s) \phi_m(z) \frac{e^{-\alpha_r(m)(r_s+r_i)}}{\sqrt{\kappa_r(m)(r_s+r_i)}} e^{j\kappa_r(m)(r_s+r_i)}. \quad (2.17)$$

Assuming that $r_s \gg r_i$, the model can be simplified, resulting in

$$p(\rho_i, z) = \sum_{m=1}^N \phi_m(z_s) \phi_m(z) \frac{e^{j(\kappa_r(m)+j\alpha_r(m))r_s}}{\sqrt{\kappa_r(m)r_s}} e^{j\kappa_r(m)r_i}, \quad i = 1, \dots, L. \quad (2.18)$$

Expanding this expression we have

$$\begin{bmatrix} p(\rho_1, z) \\ \vdots \\ p(\rho_L, z) \end{bmatrix} = \begin{bmatrix} e^{j\kappa_r(1)r_1} & \dots & e^{j\kappa_r(N)r_1} \\ \vdots & & \vdots \\ e^{j\kappa_r(1)r_L} & \dots & e^{j\kappa_r(N)r_L} \end{bmatrix} \times \begin{bmatrix} \phi_1(z_s) \phi_1(z) e^{j(\kappa_r(1)+j\alpha_r(1))r_s} / \sqrt{\kappa_r(1)r_s} \\ \vdots \\ \phi_N(z_s) \phi_N(z) e^{j(\kappa_r(N)+j\alpha_r(N))r_s} / \sqrt{\kappa_r(N)r_s} \end{bmatrix}$$

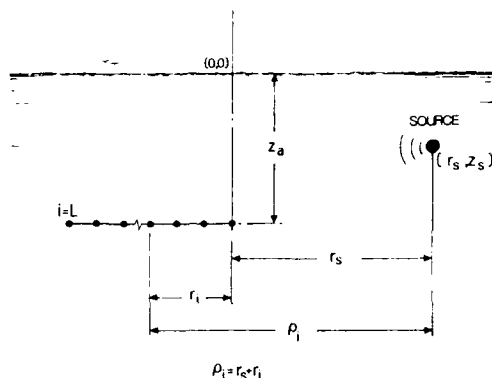


Fig. 1. Configuration of L -element array which spatially samples the radiation from the acoustic source located at depth Z , and range r_s .

which can be written succinctly as

$$\underline{p}(\underline{r}, z) = \mathbf{D}(\underline{r})\underline{\phi}(r_s, z), \quad (2.19)$$

with $\underline{p} \in \mathbb{C}^{L \times 1}$, $\mathbf{D} \in \mathbb{C}^{L \times N}$, and $\underline{\phi} \in \mathbb{C}^{N \times 1}$. \mathbf{D} is called the *direction matrix* with elements $d_{m11} = e^{j\kappa_r(n)r_m}$ and can be defined in terms of row or column vectors as

$$\mathbf{D}(\underline{r}) := [\underline{d}(\kappa_1) \dots \underline{d}(\kappa_N)] = \begin{bmatrix} \underline{d}'(r_1) \\ \vdots \\ \underline{d}'(r_L) \end{bmatrix}. \quad (2.20)$$

The measurements will be contaminated with noise in the practical case, and therefore we assume the *measurement model*:

$$\underline{p}(\underline{r}, z) = \mathbf{D}(\underline{r})\underline{\phi}(r_s, z) + \underline{\epsilon}(\underline{r}, z), \quad (2.21)$$

where $\underline{\epsilon}$ is assumed spatially white with variance $\mathbf{R}_{\epsilon\epsilon}$.

Proceeding further, let us analyse the information contained in these measurements.

Post-multiplying by the hermitian conjugate¹ and taking expected values, we have

$$E\{\underline{p}(r, z)\underline{p}^{\dagger}(r, z)\} = \mathbf{D}(r)E\{\underline{\phi}(r, z)\underline{\phi}^{\dagger}(r, z)\}\mathbf{D}^{\dagger}(r) + E\{\underline{\xi}(r, z)\underline{\xi}^{\dagger}(r, z)\}$$

or simply

$$\mathbf{R}_{pp} = \mathbf{D}(r)\mathbf{R}_{\phi\phi}\mathbf{D}^{\dagger}(r) + \mathbf{R}_{\xi\xi}. \quad (2.22)$$

Since there are precisely N modes characterizing the source, we have

$$\text{rank} [\mathbf{D}(r)\mathbf{R}_{\phi\phi}\mathbf{D}^{\dagger}(r)] = N < L. \quad (2.23)$$

Performing an eigendecomposition of \mathbf{R}_{pp} , we have that

$$\mathbf{R}_{pp} = \mathbf{E}\Lambda_{pp}\mathbf{E}^{\dagger}, \quad (2.24)$$

where \mathbf{E} is the corresponding eigenvector matrix and

$$\Lambda_{pp} = \text{diag} [\lambda_1, \dots, \lambda_L].$$

Using the measurement model we obtain

$$\Lambda_{pp} = \mathbf{E}^{\dagger}\mathbf{R}_{pp}\mathbf{E} = \mathbf{E}^{\dagger}(\mathbf{D}(r)\mathbf{R}_{\phi\phi}\mathbf{D}^{\dagger}(r))\mathbf{E} + \mathbf{E}^{\dagger}\mathbf{R}_{\xi\xi}\mathbf{E}. \quad (2.25)$$

If we further assume that ξ is i.i.d. (independent and identically distributed), then $\mathbf{R}_{\xi\xi} = \sigma^2\mathbf{I}$ and therefore it follows that

$$\Lambda_{pp} = \Lambda_{\phi\phi} + \sigma^2\mathbf{I}, \quad (2.26)$$

or

$$\begin{bmatrix} \lambda_1 & & & 0 \\ & \ddots & & \\ & & \lambda_N & \\ 0 & & & \ddots \\ & & & & \lambda_L \\ & & & & & 0 \end{bmatrix} = \begin{bmatrix} \mu_1 & & & 0 \\ & \ddots & & \\ & & \mu_N & \\ 0 & & & \ddots \\ & & & & 0 \end{bmatrix} + \begin{bmatrix} \sigma^2 & & & 0 \\ & \ddots & & \\ & & \sigma^2 & \\ 0 & & & \ddots \\ & & & & \sigma^2 \\ & & & & & 0 \end{bmatrix} \quad (2.27)$$

giving the eigenvalues

$$\lambda_i = \begin{cases} \mu_i + \sigma^2, & 1 < i \leq N \\ \sigma^2, & N < i \leq L. \end{cases} \quad (2.28)$$

¹ It is interesting to note that integrating the hermitian product of Eq. (2.21), and using the orthogonality property Eq. (2.10) of the modal functions, we have

$$\mathbf{R}_{pp} \approx \int_0^h \rho_0 \underline{p} \underline{p}^{\dagger} dz = \mathbf{D} \left[\int_0^h \rho_0 \underline{\phi} \underline{\phi}^{\dagger} dz \right] \mathbf{D}^{\dagger} + \mathbf{R}_{\xi\xi}$$

and the signal term can be expressed as $\sum_{m=1}^N \beta_m^2 \underline{d}(\kappa_m) \underline{d}^{\dagger}(\kappa_m)$, with β_m representing modal power. Here $\mathbf{R}_{\phi\phi}$ is real and the range can be obtained directly from diagonals.

This relation implies the existence of two subspaces:

- (i) The *signal* subspace spanned by the eigenvectors (modal functions) associated with the N largest eigenvalues of \mathbf{R}_{pp} .
- (ii) The *noise* subspace spanned by the eigenvectors associated with the $L - N$ smallest eigenvalues of \mathbf{R}_{pp} .

Investigating the noise subspace further we see that [12, 13]

$$(\mathbf{R}_{pp} - \sigma^2 I)\mathbf{e}_i = \mathbf{0} \quad \text{for } i = N + 1, \dots, L, \quad (2.29)$$

or using Eq. (2.22) with $\mathbf{R}_{ee} = \sigma^2 I$, we have that

$$\left(\mathbf{D}(\underline{r})\mathbf{R}_{\phi\phi}\mathbf{D}^t(\underline{r}) \right) \mathbf{e}_i = \mathbf{0} \quad \text{for } i = N + 1, \dots, L, \quad (2.30)$$

where \mathbf{e}_i is the i th vector of \mathbf{E} .

Equation (2.30) implies that the eigenvectors associated with the noise subspace are orthogonal to the signal subspace. This can be seen by assuming $\mathbf{D}(\underline{r})$ is full rank and $\mathbf{R}_{\phi\phi}$ is invertible. It then follows that

$$\mathbf{D}^t(\underline{r})\mathbf{e}_i = \mathbf{0} \quad \text{for } i = N + 1, \dots, L, \quad (2.31)$$

or equivalently, using Eq. (2.20), we have

$$[\underline{d}^t(\kappa_1), \dots, \underline{d}^t(\kappa_N)]\mathbf{e}_i = \mathbf{0}$$

or

$$\underline{d}^t(\kappa_l)\mathbf{e}_i = \mathbf{0} \quad \text{for } l = 1, \dots, N \quad \text{and } i = N + 1, \dots, L, \quad (2.32)$$

which shows the orthogonality of the signal and noise subspaces. Following Johnson [13] we define the *eigenvector constraint matrix* as

$$\mathbf{C}_{EV} = \sum_{i=N+1}^L \mathbf{e}_i \mathbf{e}_i^t = [\mathbf{e}_{N+1} \dots \mathbf{e}_L] \begin{bmatrix} \mathbf{e}_{N+1}^t \\ \vdots \\ \mathbf{e}_L^t \end{bmatrix}. \quad (2.33)$$

But since $\mathbf{e}_i^t \mathbf{e}_i = \mathbf{0}$ for $i = N + 1, \dots, L$ and $i = 1, \dots, N$, then premultiplying by \mathbf{e}_i and summing over l we have

$$\left(\sum_{l=N+1}^L \mathbf{e}_l \mathbf{e}_l^t \right) \mathbf{e}_i = \mathbf{C}_{EV} \mathbf{e}_i = \mathbf{0} \quad \text{for } i = 1, \dots, N. \quad (2.34)$$

Since $\{e_i\}$ are basis vectors spanning the signal subspace and $\{d(\kappa_i)\}$ lie within this space, we have

$$C_{EV}d(\kappa_i) = 0 \quad \text{for } i = 1, \dots, N, \quad (2.35)$$

which is the fundamental property of all eigenvector techniques. This completes the analysis of the propagation and measurement models used in this study; next we use these ideas to develop techniques to identify or estimate the required model parameters from noisy data.

3. Processor design

In this section we discuss the development of a processor designed to extract parameters of the acoustic propagation model from noisy measurement data. To motivate the approach we reconsider the propagation model of Eq. (2.18). The directional information and subsequent range information about the location of the source is contained in the wavenumbers and therefore in the phase of the measured data, since the modal functions are *real*. In fact, we can interpret the field at the array as being composed of a superposition of plane waves $e^{j\kappa_r(m)r}$ emanating from the same location and impinging upon the horizontal array as depicted in Fig. 2. Therefore the goal is to develop a processor to estimate the horizontal wavenumbers $\{\kappa_r(m)\}$ from the pressure measurement and then utilize them to estimate the range.

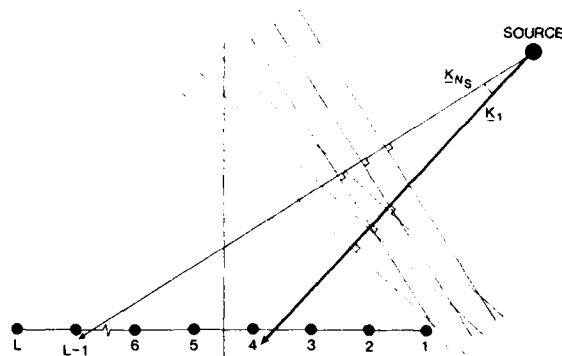


Fig. 2. Modal function plane wave-decomposition model. The modal wave numbers can be envisioned as arriving from a fictitious point source radiating plane waves with equal wavelengths but different angles.

We begin our development of the processor by first examining the idea of directional constraints and then design an optimal-constrained processor to estimate the direction-of-arrival or wavenumbers of the modal functions $\phi_m(z)$. Before we state the problem let us recall that the array pattern or spatial frequency response of an array is defined by

$$A(\kappa) = \sum_{i=1}^L a_i e^{-j\kappa' z_i} = \underline{a}' \underline{d}(\kappa), \quad (3.1)$$

where $\underline{\kappa}$ is the wavenumber vector, \underline{r}_i is the spatial position vector of the i th sensor, \underline{a} is the weight vector and \underline{d} is the direction vector.

Using this definition, we can develop *directional constraints* in terms of wavenumber $\underline{\kappa}_i$ by constraining the gain to unity in the desired direction, i.e.

$$A(\underline{\kappa}_i) = \underline{a}^t \underline{d}_i(\underline{\kappa}) = 1. \quad (3.2)$$

A constrained optimal technique requires that we select a set of weights, say $\{w_i\}$, to minimize the acoustical output power in every direction *except* that of the constraint and satisfy

$$\min_{\underline{w}} \underline{w}^t \mathbf{R}_{pp} \underline{w}$$

such that

$$\underline{w}^t \underline{d}_i(\underline{\kappa}) = 1.$$

Minimization of the augmented cost function

$$\min_{\underline{w}} \mathbf{J} = \underline{w}^t \mathbf{R}_{pp} \underline{w} + \beta \left(1 - \underline{w}^t \underline{d}_i(\underline{\kappa}) \right)$$

leads to the minimum variance distortionless response (MVDR) solution for power [8], which is given by

$$P_{\text{MVDR}}(i) = \frac{1}{\underline{d}_i^t(\underline{\kappa}) \mathbf{R}_{pp}^{-1} \underline{d}_i(\underline{\kappa})}. \quad (3.3)$$

In the eigen-decomposition approach, the directional constraint equation is chosen to be

$$\underline{w}^t \mathbf{C}_{EV}^t \underline{d}_i(\underline{\kappa}) = 1, \quad (3.4)$$

and therefore, the optimal-constrained processor must minimize:

$$\min_{\underline{w}} \mathbf{J} = \underline{w}^t \mathbf{R}_{pp} \underline{w} + \beta \left(1 - \underline{w}^t \mathbf{C}_{EV}^t \underline{d}_i(\underline{\kappa}) \right).$$

Using the chain-rule¹ of vector calculus we have

$$\nabla_{\underline{w}} \mathbf{J} = 2\mathbf{R}_{pp} \underline{w} - \beta \mathbf{C}_{EV}^t \underline{d}_i(\underline{\kappa}) = 0$$

or solving for \underline{w} we obtain

$$\underline{w} = \frac{1}{2} \beta \mathbf{R}_{pp}^{-1} \mathbf{C}_{EV}^t \underline{d}_i(\underline{\kappa}). \quad (3.5)$$

¹ The chain-rule for a, b, n -vectors is given by $\nabla_{\underline{w}} \underline{a}^t \underline{b} = (\nabla_{\underline{w}} \underline{a}^t) \underline{b} + (\nabla_{\underline{w}} \underline{b}^t) \underline{a}$ where ∇ is the gradient n -vector.

Taking the hermitian transpose and substituting it into the constraint equation, we have

$$\beta = \frac{2}{\underline{d}_i^{\dagger}(\kappa) \mathbf{C}_{EV} \mathbf{R}_{PP}^{-1} \mathbf{C}_{EV}^{\dagger} \underline{d}_i(\kappa)},$$

which gives the optimal weight vector as

$$\underline{w}_{opt} = \frac{\mathbf{R}_{PP}^{-1} \mathbf{C}_{EV}^{\dagger} \underline{d}_i(\kappa)}{\underline{d}_i^{\dagger}(\kappa) \mathbf{C}_{EV} \mathbf{R}_{PP}^{-1} \mathbf{C}_{EV}^{\dagger} \underline{d}_i(\kappa)}. \quad (3.6)$$

Substituting this expression into the corresponding cost function we have the minimum power as

$$\begin{aligned} \mathbf{J}_{min} &= \underline{w}_{opt}^{\dagger} \mathbf{R}_{PP} \underline{w}_{opt} \\ &= \left(\frac{\mathbf{R}_{PP}^{-1} \mathbf{C}_{EV}^{\dagger} \underline{d}_i(\kappa)}{\underline{d}_i^{\dagger}(\kappa) \mathbf{C}_{EV} \mathbf{R}_{PP}^{-1} \mathbf{C}_{EV}^{\dagger} \underline{d}_i(\kappa)} \right)^{\dagger} \mathbf{R}_{PP} \left(\frac{\mathbf{R}_{PP}^{-1} \mathbf{C}_{EV}^{\dagger} \underline{d}_i(\kappa)}{\underline{d}_i^{\dagger}(\kappa) \mathbf{C}_{EV} \mathbf{R}_{PP}^{-1} \mathbf{C}_{EV}^{\dagger} \underline{d}_i(\kappa)} \right). \end{aligned}$$

Or letting $P(i) = \mathbf{J}_{min}$ we have

$$P(i) = \left(\frac{\underline{d}_i^{\dagger}(\kappa) \mathbf{C}_{EV}}{\underline{d}_i^{\dagger}(\kappa) \mathbf{C}_{EV} \mathbf{R}_{PP}^{-1} \mathbf{C}_{EV}^{\dagger} \underline{d}_i(\kappa)} \right) \mathbf{R}_{PP} \left(\frac{\mathbf{R}_{PP}^{-1} \mathbf{C}_{EV}^{\dagger} \underline{d}_i(\kappa)}{\underline{d}_i^{\dagger}(\kappa) \mathbf{C}_{EV} \mathbf{R}_{PP}^{-1} \mathbf{C}_{EV}^{\dagger} \underline{d}_i(\kappa)} \right). \quad (3.7)$$

Cancelling the scalars in numerator and denominator yields

$$P(i) = \frac{1}{\underline{d}_i^{\dagger}(\kappa) \mathbf{C}_{EV} \mathbf{R}_{PP}^{-1} \mathbf{C}_{EV}^{\dagger} \underline{d}_i(\kappa)}. \quad (3.8)$$

We can simplify these expressions further by using the spectral decomposition of \mathbf{R}_{PP} , i.e.

$$\mathbf{R}_{PP} = \sum_{i=1}^L \lambda_i \underline{e}_i \underline{e}_i^{\dagger}$$

which gives

$$\mathbf{R}_{PP}^{-1} = \sum_{i=1}^L \frac{1}{\lambda_i} \underline{e}_i \underline{e}_i^{\dagger}. \quad (3.9)$$

Therefore substituting for \mathbf{R}_{PP}^{-1} we have

$$\mathbf{C}_{EV} \mathbf{R}_{PP}^{-1} \mathbf{C}_{EV}^{\dagger} = \mathbf{C}_{EV} \left(\sum_{i=1}^L \frac{1}{\lambda_i} \underline{e}_i \underline{e}_i^{\dagger} \right) \mathbf{C}_{EV}^{\dagger},$$

and from the orthogonality of the noise eigenvectors to the signal subspace we have

$$\mathbf{C}_{EV} \mathbf{R}_{pp}^{-1} \mathbf{C}_{EV}^\dagger = \sum_{i=1}^L \frac{1}{\lambda_i} (\mathbf{C}_{EV} \underline{\mathbf{e}}_i) (\underline{\mathbf{e}}_i^\dagger \mathbf{C}_{EV}^\dagger) = \sum_{i=N+1}^L \frac{1}{\lambda_i} \underline{\mathbf{e}}_i \underline{\mathbf{e}}_i^\dagger, \quad (3.10)$$

since $\mathbf{C}_{EV} \underline{\mathbf{e}}_i = \mathbf{0}$ for $i = 1, \dots, N$.

We now define the notation

$$\mathbf{C}_{EV} \mathbf{R}_{pp}^{-1} \mathbf{C}_{EV}^\dagger = \mathbf{E}_{L-N} \Lambda_{L-N}^{-1} \mathbf{E}_{L-N}^\dagger, \quad (3.11)$$

where

$$\mathbf{E}_{L-N} = [\underline{\mathbf{e}}_{N+1} \dots \underline{\mathbf{e}}_L],$$

$$\Lambda_{L-N}^{-1} = \text{diag} \left[\frac{1}{\lambda_{N+1}} \dots \frac{1}{\lambda_L} \right] = \frac{1}{\sigma^2} I_{L-N}.$$

The optimal weighting vector can be written as

$$\underline{\mathbf{w}}_{\text{opt}} = \frac{\Lambda_{L-N}^{-1} \mathbf{E}_{L-N}^\dagger \underline{\mathbf{d}}_i(\kappa)}{\underline{\mathbf{d}}_i^\dagger(\kappa) \mathbf{E}_{L-N} \Lambda_{L-N}^{-1} \mathbf{E}_{L-N}^\dagger \underline{\mathbf{d}}_i(\kappa)}, \quad (3.12)$$

and the corresponding power is

$$P_{EV}(i) = \frac{1}{\underline{\mathbf{d}}_i^\dagger(\kappa) \mathbf{E}_{L-N} \Lambda_{L-N}^{-1} \mathbf{E}_{L-N}^\dagger \underline{\mathbf{d}}_i(\kappa)}, \quad (3.13)$$

which possesses the desirable property that when $\underline{\mathbf{d}}$ is at a mode the denominator approaches zero, i.e.

$$\underline{\mathbf{d}}_i^\dagger(\kappa) \mathbf{E}_{L-N} \Lambda_{L-N}^{-1} \mathbf{E}_{L-N}^\dagger \underline{\mathbf{d}}_i(\kappa) |_{\kappa=\kappa_r(m)} \rightarrow 0 \Rightarrow P_{EV}(i) \rightarrow \infty.$$

Before we close this discussion we should mention that the dimension of the signal subspace N can be estimated using the Akaike Information Criterion (AIC) or the related Minimum Data Length (MDL) description given by [14]:

$$\text{MDL}(N) = -M \ln \left(\frac{\prod_{i=N+1}^L \lambda_i}{((L-N)^{-1} \sum_{i=N+1}^L \lambda_i)^{L-N}} \right) + \frac{1}{2} N(2L-N) \ln M, \quad (3.14)$$

where N is the dimension of the signal subspace, M is the number of data values of $P(i)$, λ_i is the i th eigenvalue of \mathbf{R}_{pp} and L is the number of sensors.

This function will indicate a minimum at the true dimension of the signal subspace (number of modes). We summarize the *eigen-decomposition approach* as follows (see Appendix A for implementation):

- (1) Estimate the covariance matrix, \mathbf{R}_{pp} from acoustic pressure measurements.
- (2) Perform a singular value decomposition (SVD) of \mathbf{R}_{pp} [16].
- (3) Using the MDL of Eq. (3.14) estimate the number of modes \hat{N} .
- (4) Estimate the power $P_{EV}(i)$ of Eq. (3.13) using $\underline{d}(\kappa)$ for various values of κ .
- (5) Choose the \hat{N} peaks of $P_{EV}(i)$ and identify the corresponding wavenumbers, $\{\hat{\kappa}_r(m)\}$, $m = 1, \dots, \hat{N}$.

Once we have the wavenumber estimates, we can extract more information by using the underlying propagation and measurement models. Since we have the estimates $\{\{\hat{\kappa}_r(m)\}, \hat{N}\}$, we can construct the corresponding full-rank direction matrix and solve the measurement model relation of Eq. (2.22) for $\mathbf{R}_{\phi\phi}$, i.e.

$$\hat{\mathbf{R}}_{\phi\phi} = \mathbf{D}^*(\hat{\kappa})[\mathbf{R}_{pp} - \hat{\sigma}^2 \mathbf{I}][\mathbf{D}^*(\hat{\kappa})]^t, \quad (3.15)$$

where

$$\mathbf{D}^*(\hat{\kappa}) = [\mathbf{D}^t(\hat{\kappa})\mathbf{W}\mathbf{D}(\hat{\kappa})]^{-1}\mathbf{D}^t(\hat{\kappa})\mathbf{W},$$

$$\mathbf{D}(\hat{\kappa}) = \mathbf{D}(\kappa)|_{\kappa=\hat{\kappa}_r(m)}, \quad m = 1, \dots, \hat{N},$$

and \mathbf{W} is a weighting matrix.

The range can be estimated directly from the modal covariance matrix by first noting that the complex vector of Eq. (2.19) can be written as

$$\underline{\phi}(r_s, z) = \begin{bmatrix} |\phi_1(r_s, z)| \angle \phi_1(r_s, z) \\ \vdots \\ |\phi_N(r_s, z)| \angle \phi_N(r_s, z) \end{bmatrix} = \begin{bmatrix} a_1(r_s, z) e^{j\kappa_r(1)r_s} \\ \vdots \\ a_N(r_s, z) e^{j\kappa_r(N)r_s} \end{bmatrix}, \quad (3.16)$$

where $a_m(r_s, z) = \phi_m(z_s)\phi_m(z)e^{-\alpha(m)r_s}/\sqrt{\kappa_r(m)r_s}$. The coefficients $\{a_m(r_s, z)\}$ are real since the modal functions are real, therefore, the horizontal range can be obtained directly from the phase of ϕ . Following the approach of Sullivan and Rameau [9] we have

$$\mathbf{R}_{\phi\phi} = \mathbf{E} \begin{bmatrix} a_1^2 & \dots & a_1 a_N e^{j(\kappa_r(1) - \kappa_r(N))r_s} \\ \vdots & & \vdots \\ a_1 a_N e^{-j(\kappa_r(1) - \kappa_r(N))r_s} & \dots & a_N^2 \end{bmatrix}, \quad (3.17)$$

where the dependence of the a 's has been suppressed for clarity. Here we have used the fact that the array is towed at a depth $z = z_a \Rightarrow \phi_m(z_a) = \phi_m(z)|_{z=z_a}$. Thus the horizontal range can be determined from the phase-dependent terms of $\mathbf{R}_{\phi\phi}$ as (see [3, 9] for details):

$$\arg(\mathbf{R}_{\phi\phi}(i, l)) = (\kappa_r(i) - \kappa_r(l))r_s - \mathbf{M}\pi, \quad (3.18)$$

where the $M\pi$ term arises from the fact that $\arg(\mathbf{R}_{\phi\phi})$ is merely the principal value of the phase, and the actual sign is unknown. Solving for r_s , we have

$$r_s(i, l) = \frac{\arg(\mathbf{R}_{\phi\phi}(i, l))}{\kappa_r(i) - \kappa_r(l)} + \frac{M\pi}{\kappa_r(i) - \kappa_r(l)}. \quad (3.19)$$

As shown in [9], by introducing a third mode, two more solutions for the range can be written $r_s(i, j), r_s(i, \kappa)$. Counting all of the multiple solutions, sorting into range bins and forming a range histogram $H(r)$, we would expect the range associated with the range bin containing the maximum number of solutions to be the estimated range. The *range estimation* algorithm is as follows:

- (1) From the estimates of $\{\{\hat{\kappa}_r(i)\}, \hat{N}\}$, estimate $\hat{\mathbf{R}}_{\phi\phi}$ from Eq. (3.15).
- (2) Using the phase of $\hat{\mathbf{R}}_{\phi\phi}$ estimate r_s using Eq. (3.19), choosing $\hat{r}_s = \max H(r)|_{r=r_s}$.

This completes the section on wavenumber and range estimation. It is interesting to note that in this scheme, which we refer to as model-based processing with identification, the structure of the model is used *implicitly* to estimate the wavenumbers and range; however, the modal functions, and hence the sound velocity profile, ocean depth and ocean bottom properties, are *not* required explicitly, since the phase contains all of the information essential for parameter estimation. To put this another way, we only assume the validity of the model but no *a priori* knowledge of the model parameters is needed. A more detailed discussion of model-based techniques with identification can be found in Candy [10]. In the next section we discuss the performance of the estimators on simulated data.

4. Simulation results

In this section we discuss the results of generating simulated data from an acoustic propagation model and estimating the wavenumbers and range using the techniques described in the previous section.

The acoustic propagation model utilizes the normal-mode solutions to the cylindrical wave equation given by Eq. (2.14). We utilized the SACLANTCEN normal-mode, far-field acoustic simulator to produce pressure measurements for a source at a horizontal range of 5 km and depth of 50 m in a shallow channel of 100 m depth. We simulated the pressure measurements available from various horizontal arrays towed at a depth of 50 m. The wavenumber estimation problem requires a high resolution because of the nature of this problem. Since the modal solution can be decomposed into a superposition of plane waves (Eq. 2.18) emanating from the same location, but with different wavenumbers, the values of these wavenumbers are close to one another. Thus we require a long array coupled with high resolution array signal processing techniques.

It is well-known from classical antenna theory that the resolution of a linear array in terms of wavenumber is approximately given by

$$\Delta\kappa = \frac{\Pi}{(L-1)\Delta}. \quad (4.1)$$

For our simulation we decided to investigate arrays of length $L = 32, 64, 128,$ and 256 elements, with a spacing of 4 m corresponding to a wavelength of approximately 8 m at 190 Hz temporal frequency and respective wavenumber resolutions of $\Delta\kappa = 0.025, 0.0125, 0.00625,$ and 0.003125 r/m at a 10-dB signal-to-noise ratio. The propagation conditions supported 9 modes.

For comparative purposes we used the conventional beamformer given by

$$P_{\text{CONV}}(i) = \underline{d}_i^t(\kappa) \mathbf{R}_{pp} \underline{d}_i(\kappa), \quad (4.2)$$

and the maximum entropy approach [8] given by

$$P_{\text{MEM}}(i) = \frac{1}{\sqrt{\underline{d}_i^t(\kappa) \underline{a} \underline{a}^t \underline{d}_i(\kappa)}}, \quad (4.3)$$

where \underline{a} is the vector of predictor coefficients obtained as solution to the Toeplitz relation

$$\hat{\underline{a}} = \hat{\mathbf{R}}_{pp}^{-1} \underline{u}_i, \quad (4.4)$$

for \underline{u} a unit vector with unity in the i th row. We also used the MVDR and EV estimators of the previous section given by

$$P_{\text{MVDR}}(i) = \frac{1}{\underline{d}_i^H(\kappa) \mathbf{E} \Lambda_{pp}^{-1} \mathbf{E}^H \underline{d}_i(\kappa)}, \quad (4.5)$$

$$P_{\text{EV}}(i) = \frac{1}{\underline{d}_i^H(\kappa) \mathbf{E}_{L-N} \Lambda_{L-N}^{-1} \mathbf{E}_{L-N}^H \underline{d}_i(\kappa)}. \quad (4.6)$$

The results of these runs are shown for the case of $L = 128$ elements in Fig. 3. Here we note the sidelobes inherent in the conventional beamformer as compared to the constrained MVDR response. The high resolution EV and MEM techniques appear to resolve even the lower frequency wavenumbers as well. We summarize the estimates in Table 1 for the 128 and 256 elements arrays (only run for conventional and MEM cases). In all cases we see that for the $L = 256$ element array the conventional beamformer is able to 'resolve' 7 of the wavenumbers while the MEM method resolves 9. As the length of the array is decreased, thereby decreasing resolution, the number of wavenumbers resolved decreases to 6, even with the high-resolution methods.

Table 1
Wavenumber estimates

True	CONV (256)	MEM (256)	CONV (128)	MLM (128)	MEM (128)	EV (128)
0.793250	0.800877	0.805002	0.808631	0.808677	0.805485	0.815943
0.791566	0.791996	0.798992	0.792760	0.792705	0.788470	0.793073
0.788795	0.780461	0.790002	0.776587	0.776541	0.776977	0.776473
0.784900	0.772512	0.780048	0.762246	0.762268	0.764956	0.762637
0.779818	0.765485	0.773006	0.749114	0.749017	0.752522	0.748516
0.773545	0.757621	0.766243	0.735531	0.735531	0.738516	0.735256
0.766049	0.750461	0.758968				
0.757337		0.752065				
0.747690		0.745875				

The effect of array length on the wavenumber estimates is clearly demonstrated by the conventional array response depicted in Fig. 4. The number of wavenumbers resolved increases from 1 ($L = 32$) to 7 ($L = 256$).

The results of the range estimation using the exact and estimated wavenumbers can now be investigated. Figures 5 to 8 show the results for various array lengths where

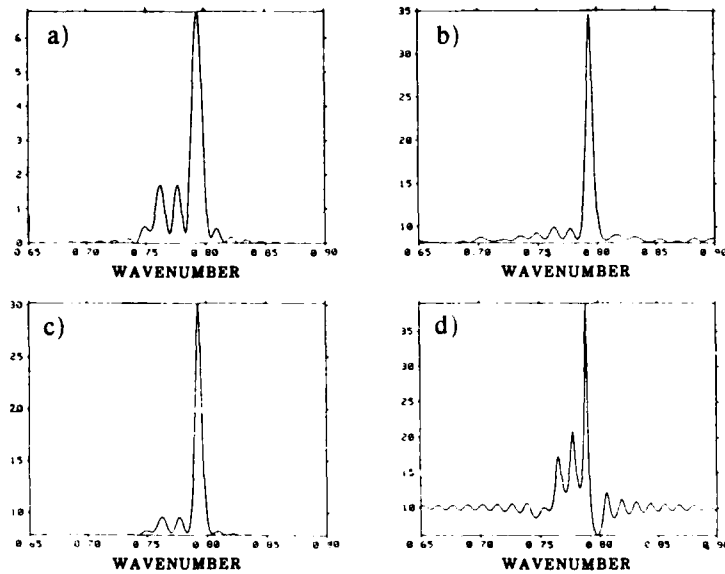


Fig. 3. Wavenumber estimates from 128 element horizontal array as estimated by four different beamformers: (a) Conventional, (b) Eigenvector, (c) Maximum Likelihood (MVDR) and (d) Maximum Entropy. The values on the ordinates are arbitrary and the abscissa is in units of wavenumbers.

the exact values of the wavenumbers, i.e. the values computed by SNAP, have been used. These values are given in Table 1 under 'True'. The four array sizes used were $L = 32, 64, 128$ and 256 elements. Since the element spacing is 4 m, these correspond respectively to absolute lengths of 124 m, 252 m and 1020 m.

There are two conclusions that can be drawn from these figures. First, that the detection performance improves with increasing array size for the first two cases (as can be seen in Figs. 5 and 6, which depict the cases for 32 and 64 elements respectively), but further increasing the array size causes a degradation in performance. This is probably a numerical problem arising in the pseudo-inverse operation on the direction matrix D of Eq. (3.15). The second conclusion to be drawn is that there is a strong positive bias in the range estimate that decreases with increasing array length. In these figures and those to follow, four plots are shown, each identified by a mode number. This number indicates the highest mode used. Thus $\text{MODES} = 5$ means that the first 5 modes were used. It can be seen that the performance is best for the lower modes in nearly all cases.

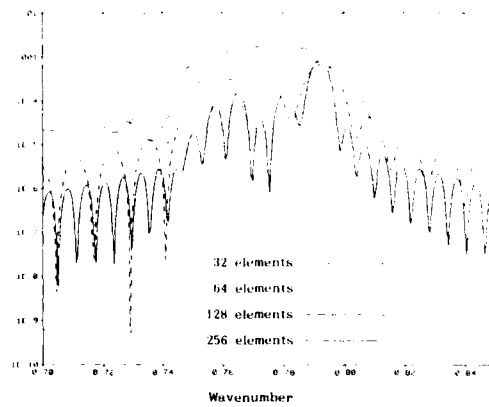


Fig. 4. Wavenumber estimation using conventional beamformer for various array lengths. The numbers in the legend indicate the number of elements, which in all cases have a spacing of approximately half of the acoustic wavelength.

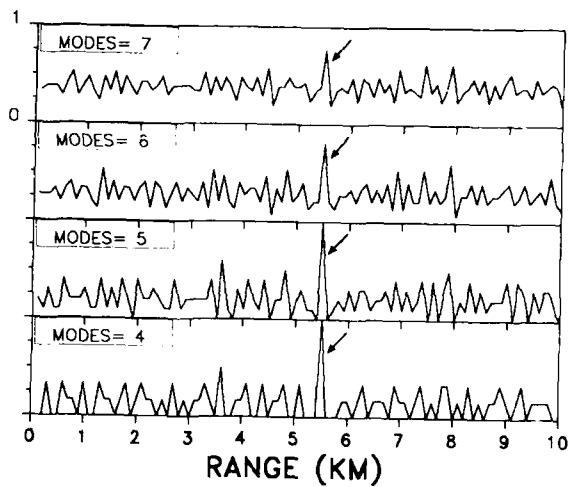


Fig. 5. Range estimator for $L = 32$ elements using exact wavenumbers.

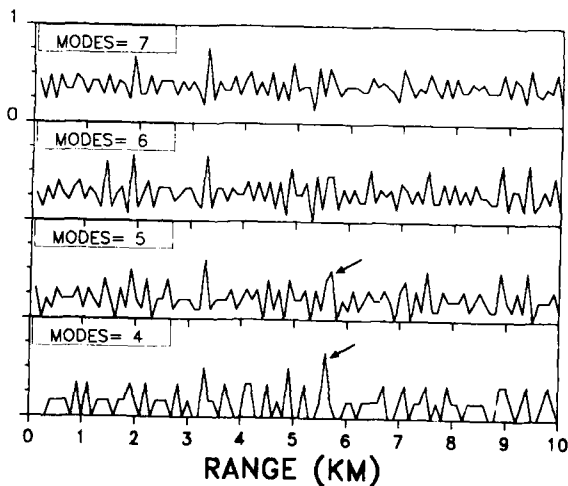


Fig. 6. Range estimator for $L = 64$ elements using exact wavenumbers.

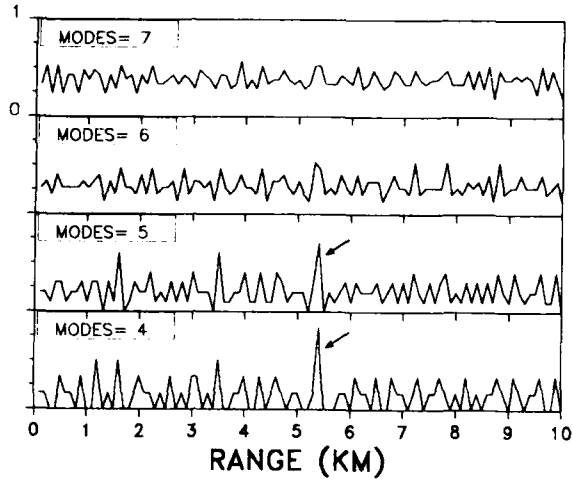


Fig. 7. Range estimator for $L = 128$ elements using exact wavenumbers.

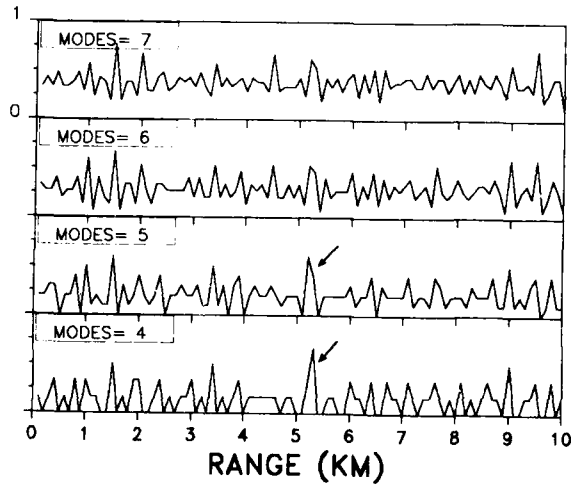


Fig. 8. Range estimator for $L = 256$ elements using exact wavenumbers.

For the case of the estimated wavenumbers, the performance, as would be expected, was not as good as that for the exact wavenumbers. In Fig. 9 the results using the wavenumbers estimated with the conventional beamformer using a 256-element array are shown. These are the values found under the column labelled CONV (256) in Table 1. Here, the bias is negative. It is presumed that this is a consequence of measurement error in the wavenumber values. Figure 10 shows the results for wavenumbers estimated with a maximum entropy beamformer (MEM (256) in Table 1). the performance is similar to that of Fig. 9 but the bias is positive.

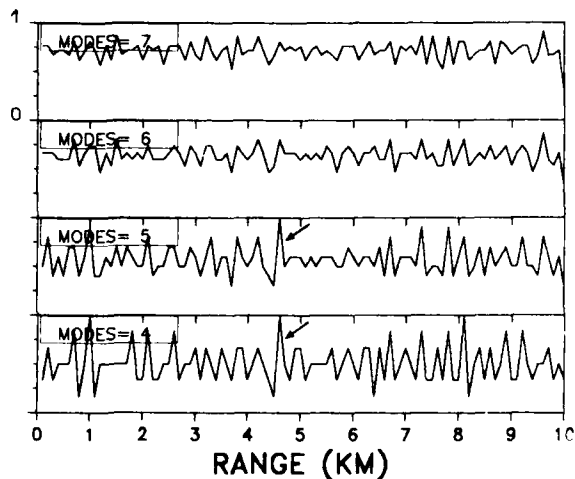


Fig. 9. Range estimator for $L = 256$ elements using wavenumbers estimated with the same array using a conventional beamformer.

The performance for the wavenumbers estimated with shorter arrays was much worse. Of the four cases tabulated in the last four columns of Fig. 3, i.e. those for the 128-element array, only those wavenumbers using the conventional beamformer give a meaningful result. This case is depicted in Fig. 11 where it can be seen that, contrary to previous results, the higher order modes seem to yield better results than the lower order modes.

The maximum likelihood and the eigenvector beamformers were not used in the 256-element case due to storage limitations.

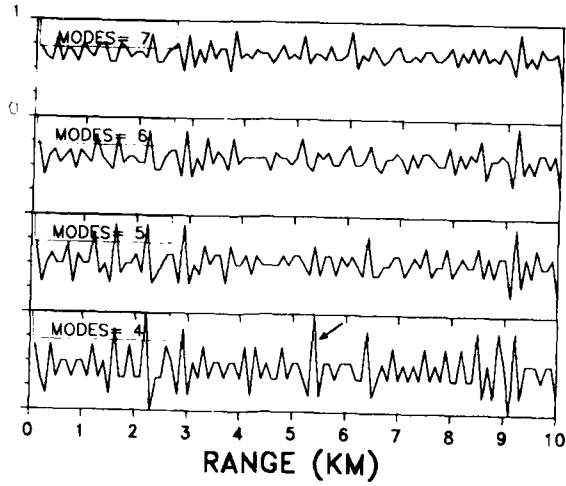


Fig. 10. Range estimator for $L = 256$ elements using wavenumbers estimated with the same array using a maximum entropy beamformer.

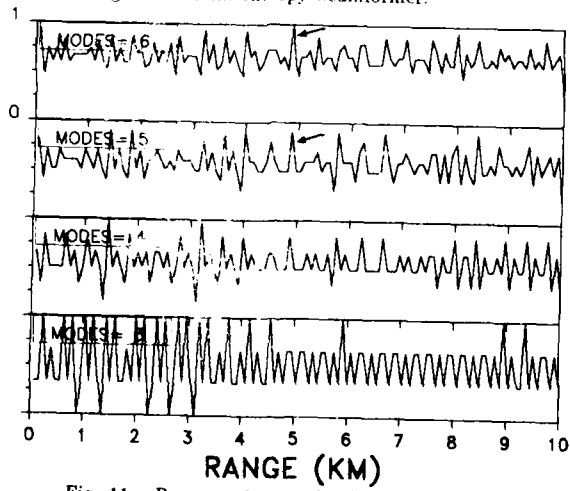


Fig. 11. Range estimator for $L = 128$ elements using wavenumbers estimated with the same array using a conventional beamformer.

5. Summary and recommendations

A model-based passive ranging scheme that requires no *a priori* knowledge of the model parameters has been developed. The feasibility of the method was demonstrated by use of synthetic data generated by a normal-mode model. Based on the results of this work, the practical difficulties appear to be connected with the measurement process itself. That is, to obtain accurate estimates of the modal wavenumbers a rather long array is necessary. In the present example an ocean depth of 100 m, which supports 9 modes at a frequency of 190 Hz, required an array at least 500 m in length. This is an unacceptable requirement for a towed array in water with a depth of only 100 m. However, with a signal with sufficient stationarity the wavenumber estimates could be made with a synthetic aperture traced out by a much shorter array, or some other model-based techniques. In this regard it should be pointed out that the process still can be carried out with *a priori* knowledge of the wavenumbers. That is, if the wavenumbers are known explicitly the data from the towed array will give a range estimate without such a prohibitive requirement in length.

The intent of this work is to demonstrate that such *a priori* knowledge is not necessary. It should also be pointed out that the horizontal array is not critical to the qualitative aspects of this approach. It is necessary only to provide the sufficient aperture for the wavenumber estimation. The vertical array cannot provide such an aperture. Any attempt to increase the aperture of the vertical array by increasing ocean depth or frequency is defeated by a concomitant increase in the number of modes that are more closely spaced in wavenumber space, thus requiring a still larger aperture.

The towed array offers an advantage over the vertical array in that the relative element positions along the range are well-known. Studies have shown that these techniques are quite sensitive to errors in the assumed element positions in the direction of the source [9]. Thus in the case of the vertical array any tilting or curving of the array can produce unacceptable errors, whereas in the towed array the spacings are mechanically fixed. However, it must be known *a priori* that the array is 'pointed' at the source. This means that, unlike the case with the vertical array, the source bearing must be determined before the range measurement is made. Of course this could be done by first towing the array across the approximate bearing of the source.

Although this study has demonstrated the feasibility of the technique, there are still some questions that must be answered to establish its practicability. First, the numerical problems that were encountered in this study must be better understood. Secondly, a sensitivity study should be carried out in order to determine the

limits on wavenumber accuracy, errors in vertical position of the elements, bearing measurement accuracy and tow-speed accuracy and stability in the case of the synthetic aperture approach. Third, studies using realistic noise fields should be carried out. Finally, and obviously, given satisfactory results of these studies, the approach should be experimentally verified.

References

- [1] HINICH, M.J. Maximum likelihood signal processing for a vertical array. *Journal of the Acoustical Society of America*, **54**, 1973: 499-503.
- [2] BUCKER, H.P. Use of calculated sound fields and matched-field detection to locate sound sources in shallow water. *Journal of the Acoustical Society of America*, **59**, 1976: 368-373.
- [3] SULLIVAN, E.J. Passive localization using propagation models. SACLANTCEN SR-117. La Spezia, Italy, SACLANT ASW Research Centre, 1987. [AD B 113 807]
- [4] FIZELL, R.G. and WALES, S.C. Source localization in range and depth in an arctic environment. *Journal of the Acoustical Society of America*, **78**, 1985: S57-S58: C'5.
- [5] FEUILLADE, C. and KINNNEY, W.A. Source localization in a waveguide using a matched-field technique. *Journal of the Acoustical Society of America*, **78**, 1985: S30: N6.
- [6] SHANG, E.C., CLAY, C.S. and WANG, Y.Y. Passive harmonic source ranging in waveguides by using mode filter. *Journal of the Acoustical Society of America*, **78**, 1985: 172-175.
- [7] CLAY, C.S. and MEDWIN, H. *Acoustical Oceanography* New York, NY, Wiley, 1977.
- [8] CAPON, J. High resolution frequency-wavenumber spectrum analysis. *Proceedings of the IEEE*, **57**, 1969: 1408-1418.
- [9] SULLIVAN, E.J. and RAMEAU, K. Passive ranging with the SNAP model: A performance study. SACLANTCEN SR-118. La Spezia, Italy, SACLANT ASW Research Centre, 1987. [AD A 183 486]
- [10] CANDY, J.V. *Signal Processing: The Model-Based Approach*, New York, NY, McGraw Hill, 1986.
- [11] HAYKIN, S., ed. *Array Signal Processing*, Englewood Cliffs, NJ, Prentice-Hall, 1984.
- [12] BIENVENU, S. and KOPP, L. Optimality of high resolution array processing using the eigensystem approach, *IEEE Transactions on Acoustics, Speech and Signal Processing*, **31**, 1983: 1235-1246.
- [13] JOHNSON, D.H. and DEGRAAF, S.R. Improving the resolution of bearing in passive sonar arrays by eigenvalue analysis. *IEEE Transactions on Acoustics, Speech and Signal Processing*, **30**, 1982: 638-647.
- [14] WAX, M. and KAILATH, T. Detection of signals by information theoretic criteria, *IEEE Transactions on Acoustics, Speech and Signal Processing*, **33**, 1985: 387-392.
- [15] JENSEN, F.B. and FERLA, M.C. SNAP: The SACLANTCEN normal-mode acoustic propagation model. SACLANTCEN SM-121. La Spezia, Italy, SACLANT ASW Research Centre, 1979. [AD A 067 256]
- [16] NOBLE, B. and DANIEL, J. *Linear Algebra*. Englewood Cliffs, NJ, Prentice Hall, 1977.

SACLANTCEN SR-138

- 28 -

intentionally blank page

Appendix A

MATLAB implementation of the algorithm

In this appendix we discuss the implementation of the wavenumber estimator using MATLAB, a matrix language software package¹ and show the corresponding MATLAB implementation of the eigen-decomposition approach of Sect. 3 of the main text. As shown in the flow diagram of Fig. A.1, the steering matrix and complex covariance matrix are calculated by separate routines and 'loaded' into the EIGSCAN routine. Once this is accomplished the EIGEN routine performs the singular value decomposition (SVD) of \mathbf{R} , i.e.

$$\mathbf{R}_{pp} = \mathbf{EV} \cdot \mathbf{SV} \cdot \mathbf{EV}' \quad (\text{A.1})$$

Next the SIGSPACE routine estimates the dimension of the signal subspace \hat{N} from the eigenvalues (SV) of \mathbf{R}_{pp} using the Akaike Information Criterion (AIC) and the Minimum Data Length (MDL) descriptions determined in the ORDER routines. Once this is accomplished the power is estimated at various steering directions using the EV routine and

$$P_{\text{EV}}(i) = \frac{1}{\mathbf{d}_i^{\dagger} \mathbf{E}_{L-N} \mathbf{\Lambda}_{L-N}^{-1} \mathbf{E}_{L-N}^{\dagger} \mathbf{d}_i} \quad (\text{A.2})$$

Next the \hat{N} peaks are determined using PEAK and sorted using SORT according to magnitude and wavenumber. Then the direction matrix is estimated, $\mathbf{D}(\hat{\kappa})$ using DIRECTION, and the signal (modal) covariance matrix \mathbf{R}_{ss} is estimated using SIGCOV. This matrix is then passed to the range estimation procedure for further processing.

Example A.1 Suppose we are given a linear array of seven elements excited by sources at $\alpha = 12^\circ, 26^\circ, 53^\circ, 75^\circ, 83^\circ$. The signal subspace is estimated as $\hat{N} = 5$ from the MDL shown in Fig. A.2, along with the corresponding bearing estimate. As can be seen in Fig. A.3, only the sources at $26^\circ, 53^\circ$ and 83° are resolved. Next the peaks are estimated, $\mathbf{D}(\hat{\kappa})$ is constructed and \mathbf{R}_{ss} is estimated.

In principle, the same approach was used to solve the passive localization problem. For completeness we include the various MATLAB routines developed.

¹ MOHLER, C. MATLAB User's Manual, University of New Mexico, May 1981.

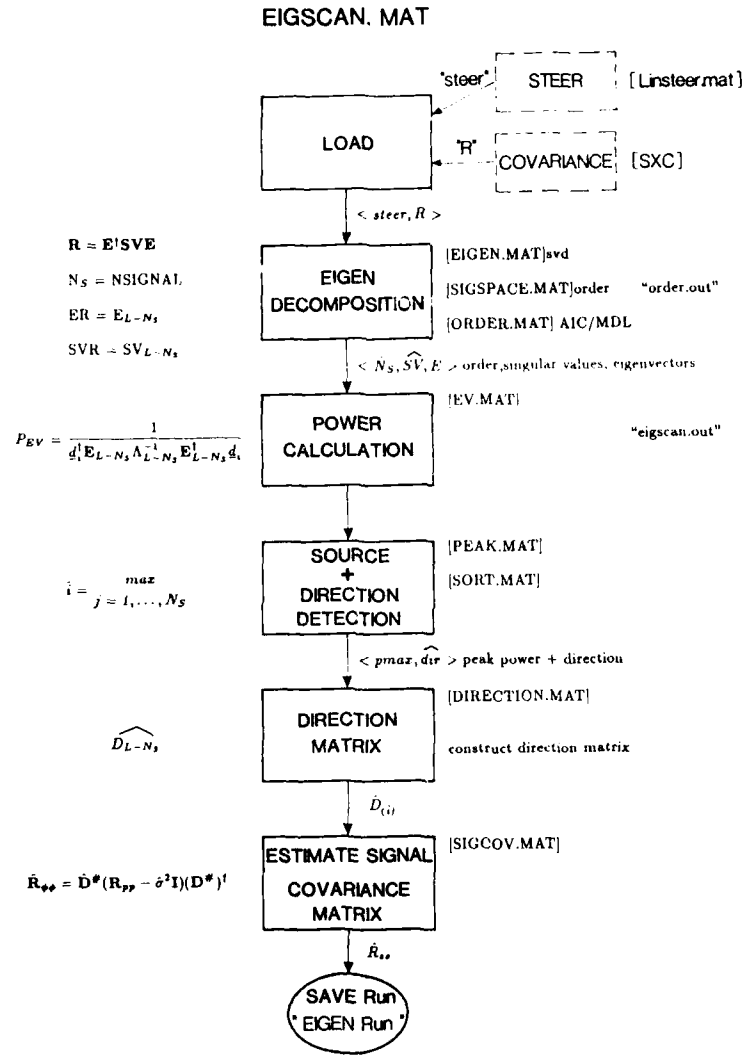


Fig. A1. MATLAB flow diagram of eigen-decomposition approach for wave-number estimator.

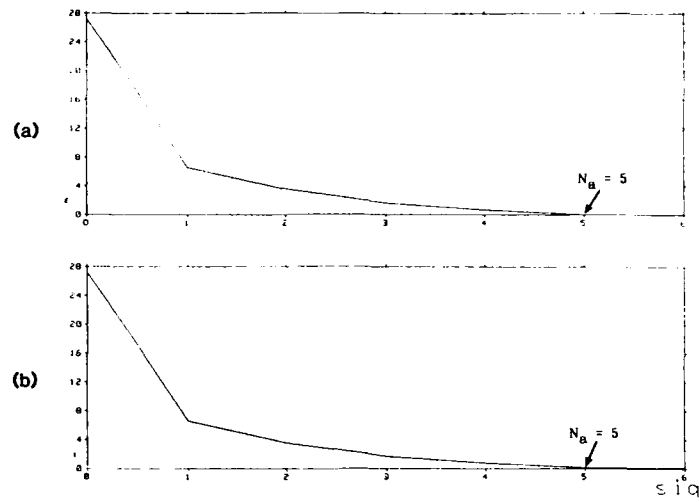


Fig. A2. Estimation of the order of the signal subspace: (a) Information criterion; (b) Minimum data length criterion.

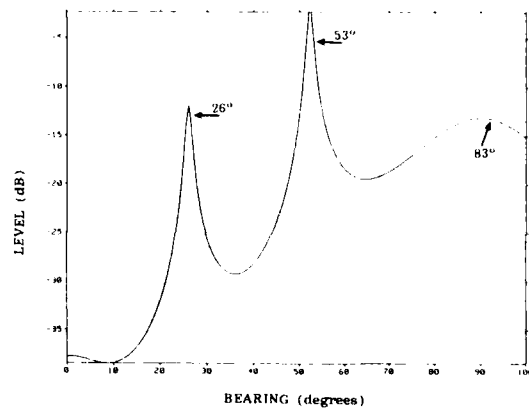


Fig. A3. Bearing estimation for the seven-element array. Only the sources at 26°, 53° and 83° are resolved.

```

////////////////////////////////////
//
//                               EIGSCAN.MAT
//
-----
// Author:           Version:           Date:
// J.V. Candy        1.1                July 21, 1987
//
-----
// This is a main routine to estimate the number of sources (nsignal) using
// EIGEN-decomposition techniques. It assumes a steering vector and
// corresponding measurement covariance matrix have been calculated
//
// Variables: (INPUT)
//          steer.hex = L x nwnum steering/direction matrix
//          wnum.dat  = nwnum-vector of steering angles
//          rpp.dat   = L x L spatial covariance matrix R
//          nelelem   = or L the number of array sensors
//          M         = Time series data length
//
// Variables: (OUTPUT)
//          p         = nwnum-vector of beam power
//          nsignal   = dimension of the signal subspace
//          pmax      = signal peak power estimates
//          dir       = estimated signal or source directions
//          Rss       = estimated signal variance matrix
//
////////////////////////////////////
//
// Load the steering and covariance matrices
//
//          load('steer.hex');
//          load('wnum.dat');
//          load('rpp.dat');
//
// Add white noise to diagonals (20 db /10)
//
//          R = conjg(R);
//          rdiag = svd(R);
//          R = R + (rdiag(1)/10)*EYE;
//          ip = 0;
//          nwnum = 251;
//          M = 501;
//          <L,L> = size(R);
//          nalpha = nwnum;
//          alpha = wnum;
//
// Perform the EIGEN-decompositions, estimate the dimension of the
// signal subspace (nsignal)
//
//          type=' Performing the Eigen-decomposition';
//          display(type)
//          exec('eigen.mat'); ..
//
// Calculate the power at various steering directions
//
//          type=' Calculating the power vs. steering directions';
//          display(type)
//          FOR n=1:nwnum, ..
//              s=steer(:,n); ..
//              exec('ev.mat'); ..
//              p(n)=10*(log(pev)/log(10)); ..
//          END, ..

```

SACLANTCEN SR-133

```
//  
// Output the results  
//  
type=' Power versus Direction Plot:';  
display(type)  
plot(wnum,p)  
short e  
print('eigscan.out',real(p));  
//  
// Detect the peaks and directions  
//  
type=' Peak Detection:';  
display(type)  
FOR n=1:nsignal, ..  
pmax(n)=-1e+12; ..  
dir(n) = 0; ..  
END, ..  
//  
diff(1)=p(1); ..  
FOR n=1:nwnum-1, ..  
exec('peak.mat'); ..  
END, ..  
//  
type=' Total number of peaks detected:';  
display(type)  
ip, ..  
//  
// Set the dimension of the signal space to the number of detected  
// peaks---or problems will evolve  
nsignal=ip;  
//  
//  
FOR n=1:ip, ..  
exec('sort.mat'); ..  
END,..  
//  
// Output the source peaks and corresponding directions  
//  
type=' The source peaks and directions are:';  
display(type)  
<real(pmax),dir>, ..  
//  
// Estimate the direction matrix and signal covariance matrix  
//  
type=' The direction matrix is:';  
display(type)  
exec('direction.mat');  
//  
//  
type=' The signal covariance matrix is:';  
display(type)  
exec('sigcov.mat');  
//  
// Save the results  
//  
save('eigen.run')
```


SACLANTCEN SR-138

```
///
///
///                                     PEAK.MAT
///
/// This is a routine to obtain the peaks of a given signal using forward
/// differences and checking for sign changes---it saves the peaks and
/// corresponding abscissa values.
///
/// Variables: (INPUT)
///
///         p      = calculated power from EV method
///         alpha  = wavenumber, bearing of steered beam
///
/// (OUTPUT)
///
///         peak   = nsignal-vector of max power
///         absic  = nsignal-vector of directions (wvno, bearing)
///
diff(n+1)=real(p(n+1)-p(n)); ..
IF diff(n+1)>0; ..
  IF diff(n)<0; ..
    ip = ip+1; ..
    peak(ip)=p(n+1); ..
    absic(ip)=alpha(n+1); ..
  ELSE, ..
ELSE, ..
IF diff(n+1)<0; ..
  IF diff(n)>0; ..
    ip = ip+1; ..
    peak(ip)=p(n+1); ..
    absic(ip)=alpha(n+1); ..
  ELSE, ..
ELSE, ..

///
///                                     SORT.MAT
///
/// This is a routine to sort values of a function "p(n)" and store
/// the "nsignal" largest in ascending order along with their
/// corresponding abscissa values in dir.
///
/// Variables: (INPUT)
///
///         peak   = calculated power from EV method
///         nsignal = dimension of signal subspace
///         absic  = wavenumber, bearing of steered beam
///
/// (OUTPUT)
///
///         pmax   = nsignal-vector of max power in ascend order
///         dir    = nsignal-vector of directions (wvno, bearing)
///
il=0; ..
FOR i=1:nsignal, ..
  IF peak(i) > pmax(i); ..
    il = i; ..
  ELSE, ..
END, ..
FOR k=1:il-1, ..
  pmax(k)=pmax(k+1); ..
  dir(k)=dir(k+1); ..
END, ..
IF il>0, ..
  pmax(il)=peak(i); ..
  dir(il)=absic(i); ..
ELSE, ..
```


Initial Distribution for SR-138

Ministries of Defence

JSPHQ Belgium	2
DND Canada	10
CHOD Denmark	8
MOD France	8
MOD Germany	15
MOD Greece	11
MOD Italy	10
MOD Netherlands	12
CHOD Norway	10
MOD Portugal	2
MOD Spain	2
MOD Turkey	5
MOD UK	20
SECDEF US	68

NATO Authorities

Defence Planning Committee	3
NAMILCOM	2
SACLANT	3
SACLANTREPEUR	1
CINWESTLANT/	
COMOCEANLANT	1
COMSTRIKFLTANT	1
CINCIBERLANT	1
CINCEASTLANT	1
COMSUBACLANT	1
COMMAIREASTLANT	1
SACEUR	2
CINCNORTH	1
CINC SOUTH	1
COMNAVSOUTH	1
COMSTRIKFORSOUTH	1
COMEDCENT	1
COMMARARMED	1
CINCHAN	3

SCNR for SACLANTCEN

SCNR Belgium	1
SCNR Canada	1
SCNR Denmark	1

SCNR Germany	1
SCNR Greece	1
SCNR Italy	1
SCNR Netherlands	1
SCNR Norway	1
SCNR Portugal	1
SCNR Turkey	1
SCNR UK	1
SCNR US	2
SEC GEN Rep. SCNR	1
NAMILCOM Rep. SCNR	1

National Liaison Officers

NLO Canada	1
NLO Denmark	1
NLO Germany	1
NLO Italy	1
NLO UK	1
NLO US	1

NLR to SACLANT

NLR Belgium	1
NLR Canada	1
NLR Denmark	1
NLR Germany	1
NLR Greece	1
NLR Italy	1
NLR Netherlands	1
NLR Norway	1
NLR Portugal	1
NLR Turkey	1
NLR UK	1

Total external distribution	241
SACLANTCEN Library	10
Stock	29
Total number of copies	280